Earth and Planetary Science Letters 556 (2021) 116704

Contents lists available at ScienceDirect

Earth and Planetary Science Letters

www.elsevier.com/locate/epsl

Mg isotope evidence for restriction events within the Paleotethys ocean around the Permian-Triassic transition

Zhongya Hu [a,b], Weiqiang Li [b,*], Hua Zhang [c,d,*], Karl Krainer [e], Quan-feng Zheng [c,d], Zhiguang Xia [b], Wenxuan Hu [b], Shu-zhong Shen [b,d,f]

[a] State Key Laboratory of Marine Geology, School of Ocean and Earth Science, Tongji University, Shanghai, China
[b] State Key Laboratory for Mineral Deposits Research, School of Earth Sciences and Engineering, Nanjing University, Nanjing, Jiangsu, China
[c] State Key Laboratory of Palaeobiology and Stratigraphy, Nanjing Institute of Geology and Palaeontology, Chinese Academy of Sciences, Nanjing, Jiangsu, China
[d] Center for Excellence in Life and Paleoenvironment, Chinese Academy of Sciences, Nanjing, Jiangsu, China
[e] Institute of Geology and Paleontology, University of Innsbruck, Austria
[f] Key Laboratory of Continental Collision and Plateau Uplift, Institute of Tibetan Plateau Research and Center for Excellence in Tibetan Plateau Earth Sciences, Chinese Academy of Sciences, Beijing 100101, China

ARTICLE INFO

Article history:
Received 10 August 2020
Received in revised form 20 November 2020
Accepted 1 December 2020
Available online 5 January 2021
Editor: F. Moynier

Keywords:
dolomite
Mg isotopes
Permian–Triassic transition
Paleotethys
restriction

ABSTRACT

The Permian–Triassic transition witnessed the largest mass extinction event in Earth's history, multiple mechanisms have been proposed to explain the cause of this catastrophe, however, relatively less attention has been paid to the paleogeography and major element chemistry of seawater and its possible link to mass extinction during this interval. Syndepositional massive marine dolostones could record the Mg isotope signature of contemporaneous seawater that hold clues of ancient Mg cycling. In this study, we investigated Mg isotopes of dolomite from three widely spaced carbonate sections in the Paleotethys to trace oceanic Mg cycling during this critical period. The latest Permian dolostones from all studied sections have similar δ^{26}Mg values around -2.1 ± 0.1‰. However, a remarkable and consistent increase in $\delta^{26}Mg_{dolomite}$ across the extinction interval occurred in both eastern and western margins of the Paleotethys. The results suggest that δ^{26}Mg of seawater in Paleotethys fluctuated by 0.4‰ within ~750 kyr across the Permian-Triassic transition. Modeling reveals that the high rate of change in $\delta^{26}Mg_{seawater}$ required an extremely short residence time for seawater Mg. This is attributed to dramatically intensified dolomitization in a restricted oceanic environment, with Mg isotope evidence revealing that the Paleotethys Ocean experienced transient restriction events, in association with radical changes in the major cation composition of seawater, around the end-Permian mass extinction event (EPME).

1. Introduction

More than 81% of marine species were wiped out within 61±48kyr at the Permian–Triassic transition, marking the greatest extinction event in Earth's history (Burgess et al., 2014; Fan et al., 2020). The triggers and kill mechanisms of this largest mass extinction event remain controversial, with different causes proposed, including sea-level changes (Yin et al., 2014), rapid global warming (Chen et al., 2016; Joachimski et al., 2012), ocean acidification (Clarkson et al., 2015), oceanic anoxia or euxinia (Zhang et al., 2018, 2020), and catastrophic soil erosion from continents following terrestrial ecosystem collapse (Sephton et al., 2005), which are mostly interpreted to be caused by the eruption of the Siberian Traps large igneous province (SLIP) (e.g., Burgess and Bowring, 2015). The EPME was accompanied by significant negative δ^{13}C excursions in carbonates globally (Shen et al., 2013; Xie et al., 2007). More recently, significant changes of stable isotope ratios of certain metals including Ca and U in carbonates have also been reported to correlate with the mass extinction (e.g., Zhang et al., 2018; Wang et al., 2019).

Magnesium isotopes are an emerging isotopic tool that could be powerful for tracing global Mg cycling, which is directly coupled with the cycling of CO_2 through continental weathering and carbonates precipitation. Because precipitation of carbonates is associated with large Mg isotope fractionations, Mg isotopes in seawater are responsive to changes in seawater chemistry, on both large and small temporal scales (Bialik et al., 2018; Li et al., 2015). Among the different types of carbonate sediments, massive dolo-

* Corresponding authors.
E-mail addresses: liweiqiang@nju.edu.cn (W. Li), hzhang@nigpas.ac.cn (H. Zhang).

https://doi.org/10.1016/j.epsl.2020.116704
0012-821X/

stones (particularly those that contain stoichiometric dolomite) have been shown to be robust against post-depositional overprinting as archive for C-Mg isotope signatures (Chang et al., 2020; Hu et al., 2017; Mueller et al., 2020). Despite the fact that dolomite is commonly viewed as a diagenetic product, dolomitization of Ca-carbonate precursors at tropical temperature (i.e., 30 °C) could occur within several kyr (Kaczmarek and Thornton, 2017), which is almost contemporaneous from a geological perspective. Dolomite may have different origins and not all dolomite can be used as seawater δ^{26}Mg recorder, nonetheless, seawater can provide sufficient Mg for extensive massive sedimentary dolostone units, and recent studies have demonstrated that a large proportion of dolostone units are "seawater-buffered" in terms of Mg isotopes (Higgins et al., 2018). Dolomite Mg isotopes have exhibited great potential to trace marine environmental changes, such as the restriction of the Cretaceous carbonate platform (Bialik et al., 2018) and Proterozoic ocean anoxia (Shen et al., 2016).

To better understand the marine environmental changes around the EPME from a perspective of major metal element (Mg) in seawater, we performed a systematic investigation on Mg isotopes in syndiagenetic dolostones from three carbonate sections with high-resolution biostratigraphic constrained. These sections are located at the eastern and western margins of the Paleotethys ocean respectively, and have been well documented for conodont biostratigraphy, chemostratigraphy, and geochronology (Cao et al., 2010; Holser et al., 1989; Wang et al., 2019; Zhang et al., 2020). The new data provide key constraints on the Mg cycling during the Permian-Triassic transition, and shed novel insights into the link between oceanic environment changes (i.e., restriction of the Paleotethys ocean) and the EPME.

2. Geological background and samples

During the end-Permian to early Triassic time interval, the major global paleogeographic units on earth included the supercontinent Pangea, Paleotethys and Panthalassa (Fig. 1A) (e.g., Yin et al., 2014). The vast Paleotethys Ocean was surrounded by Pangea in the west, the Siberian Plate in the north, the Gondwanaland in the south and Asiatic Hunic terranes within the eastern and southern parts of the ocean (Fig. 1A), which included the Cimmerian, South China, and North China blocks.

The western margin of the Paleotethys Ocean is represented by the extensively-studied Gartnerkofel-1 (GK-1) drill-core from the north slope of Mount Gartnerkofel in the Carnic Alps of southern Austria (Fig. 1A, Appendix Fig. S1A). During the late Permian, the studied area was located at a marginal basin of the western Paleotethys on an eastward-dipping homoclinal ramp and the sediments of the Gartnerkofel Core were deposited in a stable inner shelf environment (Holser et al., 1989). The core includes the upper Permian Bellerophon Formation (331–231 m) and Lower Triassic Werfen Formation (231–57 m) (Holser et al., 1989). The carbonates of the GK-1 core are predominantly dolomite. Almost all the dolostone samples are composed of dolomicrite and fine-crystalline dolomites (Fig. 2A), with dull red luminescence under cathodoluminescence (CL) microscope (Fig. 2D), and no signs of overgrowth and recrystallization are observed (Appendix Fig. S2). The dolomite is interpreted to be of syndiagenetic origin (Boeckelmann and Magaritz, 1991). The strata in the GK-1 core can be correlated with the outcrop sections nearby (Posenato, 2019), as well as the Meishan GSSP section using conodont biostratigraphy, $\delta^{13}C_{carb}$ chemostratigraphy (Holser et al., 1989; Shen et al., 2013; Rampino et al., 2020), and cyclostratigraphy (Rampino et al., 2000). This allows the chronology of the GK-1 core to be well correlative with the Meishan GSSP section with high-precision zircon U–Pb ages (Burgess et al., 2014) (Fig. 3). The average accumulation rate of dolostone in the GK-1 core was ~10 cm/kyr (Rampino et al., 2000). Using this rate, the estimated duration of the negative $\delta^{13}C_{carb}$ excursion recorded in the GK-1 core is 470 kyr, which is consistent with that from the Meishan GSSP section based on U–Pb ages (455 kyr; Appendix Fig. S3). A total of 78 carbonate samples from the GK-1 core were analyzed for Mg isotopes (Appendix Table S2).

The dolomitized carbonate profiles encompassing the Permian-Triassic boundary (PTB) in the eastern margin of Paleotheys are represented by the Yanggudong (YGD) section from the northeast Sichuan Basin of the upper Yangtze platform (Cao et al., 2010) and the Dajiang section in the Nanpanjiang Basin of South China (Kelley et al., 2017) (Fig. 1A, Appendix Fig. S1B). The major part of Sichuan Basin was a large intra-oceanic carbonate platform from Sinian to middle Triassic (Appendix Fig. S1B; Zhao et al., 2015). The Yanggudong section was located on the northeastern margin of the carbonate platform, bordering to a trough (Appendix Fig. S1B). In the study area, the sedimentary facies varied from reef to oolitic shoal complex during Lopingian to Early Triassic (Zhao et al., 2015). The strata in the Yanggudong section comprise the Lopingian Changhsing Formation and Lower Triassic Feixianguan Formation (Cao et al., 2010). The lithological boundary is distinct in the outcrop, where the dark gray bioclastic limestone of the Changhsing Formation contrasts with the light yellow dolostone of the Feixianguan Formation (Appendix Fig. S2-A). This sharp lithological change across the PTB interval is ubiquitous in the region as revealed by the widely distributed oil exploration boreholes (Wang et al., 2015). The dolostones in the Feixianguan Formation are mainly composed of dolomicrite and fine-crystalline dolomites (Fig. 2B). The dolomite also displays dull red luminescence under CL microscope (Fig. 2E). The dolostones are interpreted to form via the reflux dolomitization semi-closed lagoons in the intra part of the platform in an arid climate that persisted in the northeast Sichuan Basin during the earliest Triassic (Zhao et al., 2015). The first occurrence of *Hindeodus parvus* was found 1.5 m above the lithological boundary at the Yanggudong section, where a smooth negative carbon isotope excursion also reaches its lowest point, indicating that the lowermost 1.5 m of dolostone in the section was deposited during the end-Permian period (Cao et al., 2010).

The Dajiang section was located at an isolated shallow marine carbonate platform in Great Bank of Guizhou (GBG) in the Nanpanjiang Basin (Kelley et al., 2017). Due to a rapid drowning event in the Lopingian identified in GBG, the seawater was interpreted to be deeper than the area of GK-1 core (Kelley et al., 2017). Dolomitization during Permian to Triassic transition period in GBG mainly occurred in the platform interior, where the marine environment was dominated by a semi-restricted shallow carbonate platform (Kelley et al., 2017). The Dajiang section is partly dolomitized and has well constrained chemostratigraphy and biostratigraphy (Joachimski et al., 2012; Wang et al., 2019). The Permian-Triassic succession at Dajiang comprises the Wuchiaping Formation (Wuchiapingian to Changhsingian) and Daye Formation (Changhsingian to Griesbachian). The lowermost part of Daye Formation is a 20-m-thick microbialite, which has a distinct contact with the underlying Wuchiaping Formation (Wang et al., 2019). And the first occurrence of the conodont *Hindeodus parvus* had been identified within the microbialite interval (Wang et al., 2019). The dolomite-bearing carbonate samples show medium crystalline texture microscopically (Fig. 2C), however, the dolomite crystals do not display overgrowth or hydrothermal rims (Fig. 2F, Appendix Fig. S2), which commonly show bright luminescence under CL microscope. The medium crystalline texture of dolomite in the Dajiang section was interpreted to be the result of carbonate recrystallization and neomorphism in rock-buffered conditions, and the carbonate minerals have preserved primary signals, based on detailed analyses of the $\delta^{44/40}$Ca, $\delta^{88/86}$Sr, and $^{87}Sr/^{86}Sr$ records of bulk samples from the section (Wang et al., 2019).

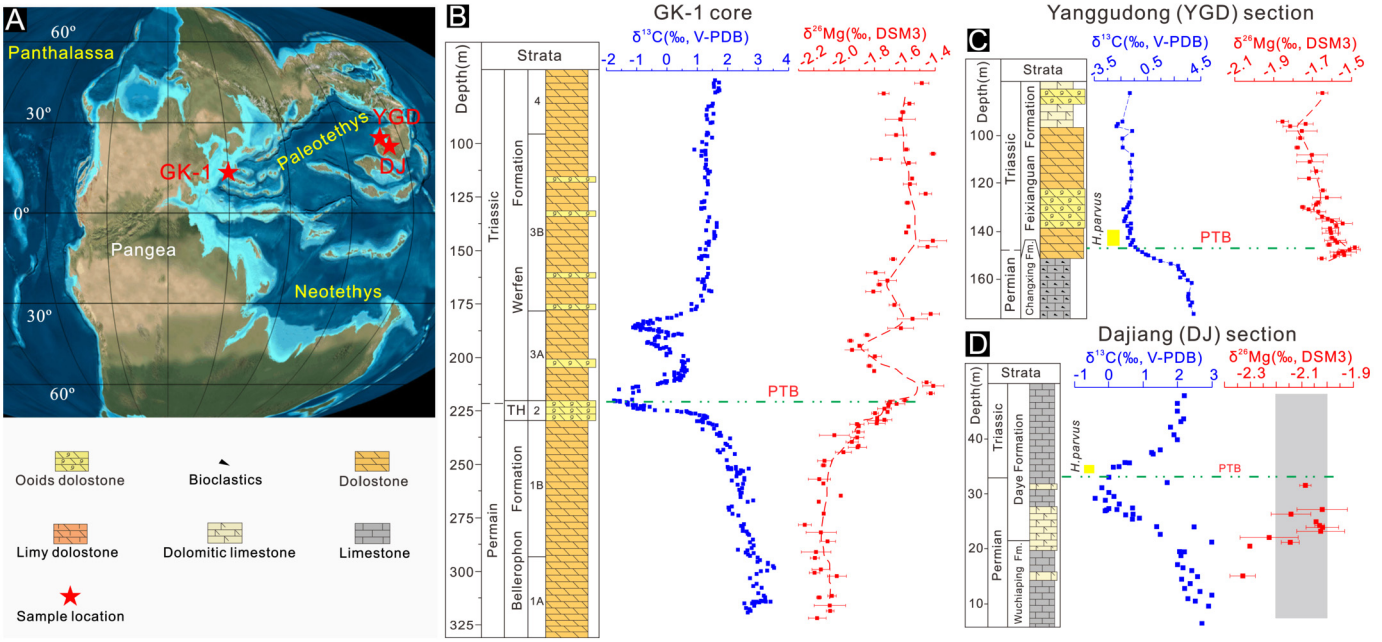

Fig. 1. (A) Global paleogeography at ~252 Ma and the location of studied sections, the base map is from Ron Blakey (http://jan.ucc.nau.edu/~rcb7/); (B)-(D) Lithological and C-Mg isotopic variations of carbonates along the studied sections in Paleotethys. In Fig. 1B, "TH" represented the Tesero Member, which is the lowermost member of the Werfen Formation, and the lithologic boundary between the Bellerophon Formation and the Werfen Formation is at the base of the Tesero Member. The $\delta^{13}C$ values of carbonate in Dajiang section are from Wang et al. (2019).

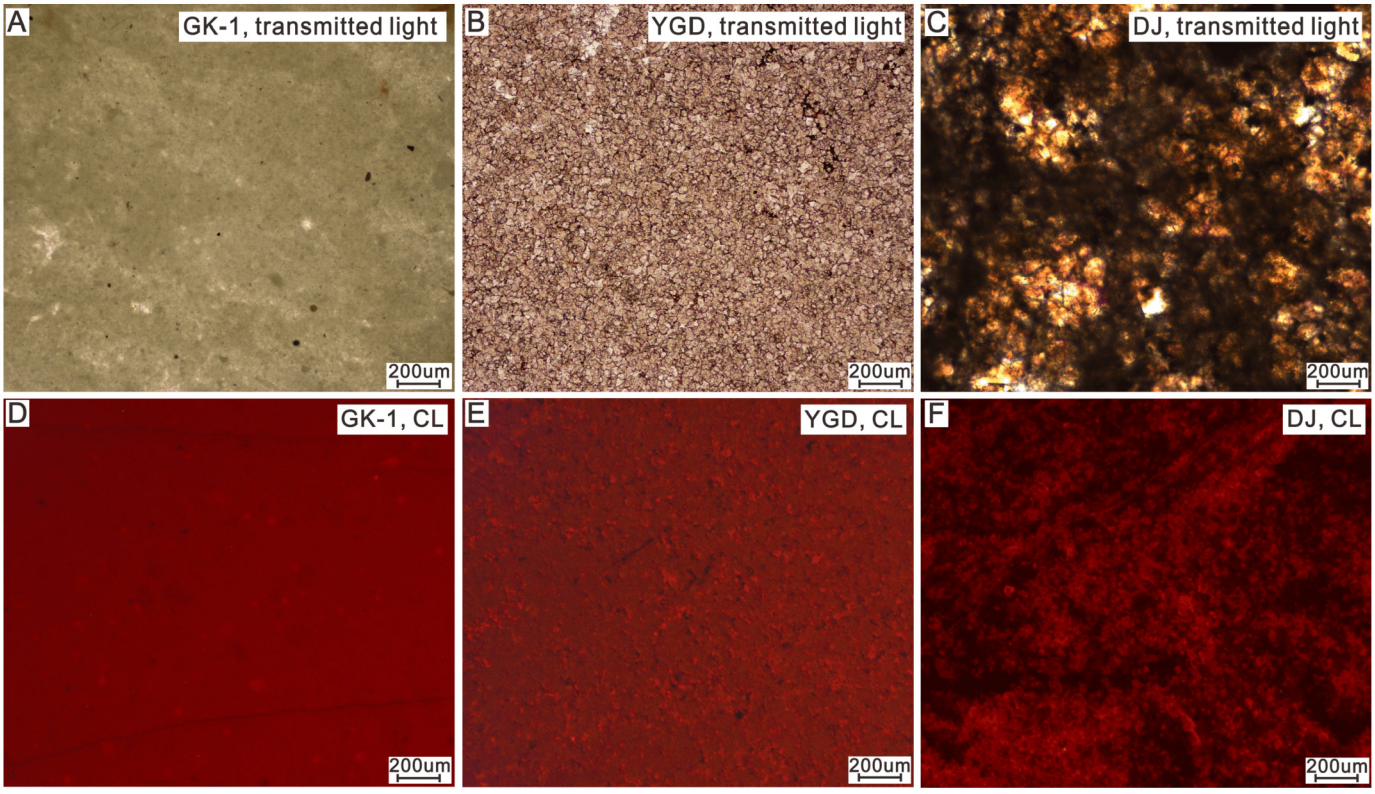

Fig. 2. Photographs showing the petrographic characteristics of representative dolomite in the studied sections. (A) fine-crystalline dolostone in GK-1 core, 149.22 m; (B) fine-crystalline dolostone in Feixianguan Formation in Lower Triassic in Yanggudong (YGD) section, 124.5 m; (C) the calcareous dolostones in microbialite of Wuchiaping Formation in Dajiang (DJ) section, 20.84 m; (D) the Cathodoluminescence photograph of the carbonate in Fig. 2A; (E) the Cathodoluminescence photograph of the dolomites in Fig. 2B; (F) the Cathodoluminescence photograph of the dolomites in Fig. 2C.

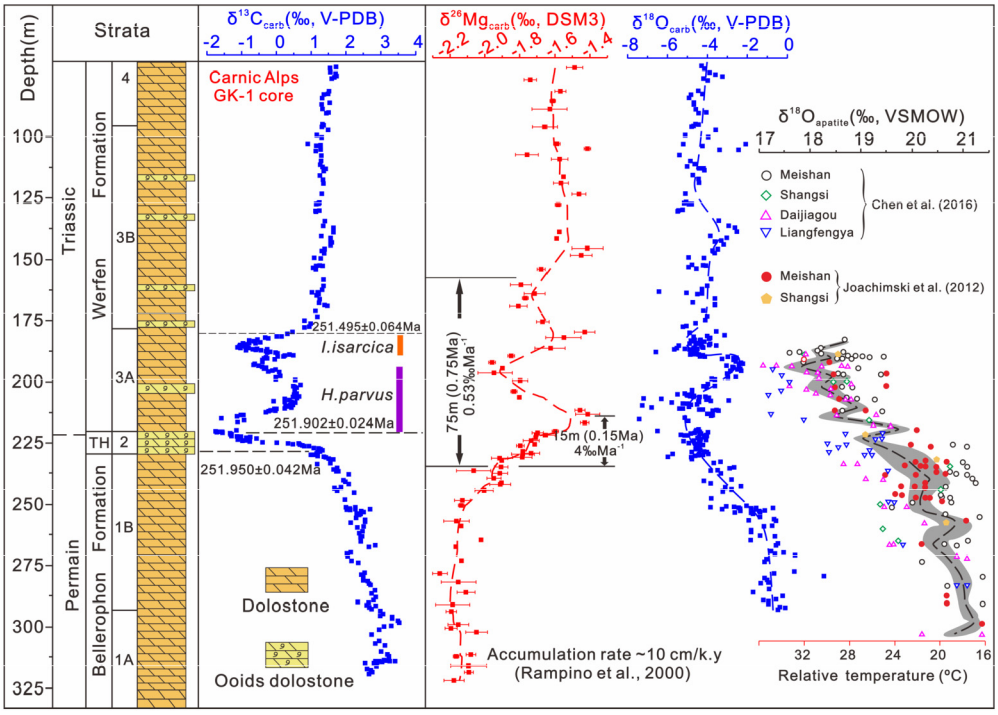

Fig. 3. The stratigraphy, geochronology and C-O-Mg isotope chemostratigraphy of the GK-1 core. The high-resolution C and O isotopes are from Holser et al. (1989). The conodont data are from Zhang et al. (2020). The temperature changes around P-T transition period that inferred from oxygen isotopes data in the conodonts apatite (the gray shadow) are from Chen et al. (2016) and Joachimski et al. (2012). (For interpretation of the colors in the figure(s), the reader is referred to the web version of this article.)

3. Analytical methods

3.1. Carbon and oxygen isotope analyses

Analyses of carbon and oxygen isotopes were performed on a Thermo Finnigan Delta-V Plus continuous flow isotope ratio mass spectrometry (IRMS) at State Key Laboratory for Mineral Deposits research, Nanjing University. Approximately 100 μg of carbonate powder was reacted with orthophosphoric acid for >12 h at 70 °C to fully transform the CO_3^{2-} into CO_2 in a gas bench that is connected to the IRMS. The C-O isotopes were presented in per mil relative to the V-PDB standard in δ notation. Following the method used by Wang et al. (2020), the standard sample GBW-04405 ($\delta^{13}C$: 0.57 ± 0.03‰, $\delta^{18}O$: −8.49 ± 0.13‰) was measured during the analysis to monitor the precision (Wang et al., 2020), and the external reproducibility was better than 0.2‰ (standard deviation, 1SD) for both $\delta^{13}C$ and $\delta^{18}O$.

3.2. Magnesium isotope analyses

Each bulk sample was powdered in a pre-cleaned agate mortar and about fifty milligrams of the powder was weighed and subsequently dissolved in 5 mL 4.5 N HNO_3 in a Teflon beaker as the stock solution. Mg fraction of each sample was recovered using two ion exchange columns that have been detailed in Hu et al. (2017). After the treatments, matrix elements were less than 1% of Mg and recovery was greater than 98%.

A 1 ppm Mg-solution in 2% HNO_3 was measured using a Thermo Fisher Scientific Neptune Plus MC-ICP-MS. The instrument was running at medium-mass-resolution mode, using a 100 μL/min self-aspirating nebulizer and a double-pass glass spray chamber. Standard-sample-standard bracketing was used for mass bias correction, the concentration of samples typically matched the in-house standard to better than ±10%. The typical internal precision (2 standard error or 2 SE) was better than ±0.04‰ for $^{26}Mg/^{24}Mg$ and ±0.02‰ for $^{25}Mg/^{24}Mg$. Based on repeat analyses of multiple Mg standard solutions, the long-term external reproducibility is better than ±0.1‰ (Appendix Table S1). Pure Mg solution of Cambridge1 and DSM3 were measured to monitor the accuracy of Mg isotope analyses. To verify the accuracy of chemical procedure, IAPSO seawater standard and USGS rock standards were processed along with samples in the ion-exchange procedure. All measured data were normalized to the international Mg isotope standard (DSM3) using conventional δ notation to express per thousand deviations. The measured $\delta^{26}Mg$ values of the standard samples well match the published values within ±0.05‰ (Appendix Table S1).

3.3. Mineral analyses

Powder X-ray diffraction analysis of bulk sample was performed on a Rigaku Rapid II dual-source X-ray Diffractometer, using a rotating anode Mo target X-ray source (Mo $K\alpha = 0.714$ Å) running at 40 kV and 100 mA. The instrument is equipped with an imaging plate, and 5 minutes exposure was used for each sample. Intensities of (104) peaks for calcite and dolomite were obtained from the XRD spectrum and the relative abundance of dolomite and calcite in bulk rocks was estimated from the intensities of the (104) peaks. The Mg contents (or stoichiometry) of calcite and dolomite were calculated following Zhang et al. (2010).

4. Results

Bulk rock XRD analyses of the GK-1 drilling core indicate the carbonate is mainly composed of dolomite, with dolomite weigh percentage mostly >90% (Appendix Table S2). The dolomite samples generally have uniform d_{104} values of around 2.883 (Appendix Table S2-2), which correspond to near-stoichiometric, ~50.0mol% $MgCO_3$ in the dolomite. In the drilling core, the late Permian dolostones have a tight distribution of $\delta^{26}Mg$ values that cluster at −2.1±0.1‰ (Fig. 1A), until the end-Permian, when $\delta^{26}Mg$ of the dolomite increased to −1.6±0.2‰ (Fig. 1A). This increase in $\delta^{26}Mg$ is mirrored by the decrease in $\delta^{13}C$ that marks the EPME. Two

phases of fluctuations in δ^{26}Mg with a magnitude of 0.5‰ occurred between 251.950±0.042 Ma and 251.495±0.064 Ma (Fig. 3), which correspond to the fluctuations of δ^{13}C in the Meishan section (Xie et al., 2007; Burgess et al., 2014), the first of which marked the EPME as indicated by the first sharp negative δ^{13}C excursion around Bed 24 top of the Meishan GSSP section (Burgess et al., 2014; Rampino et al., 2000), and the second is at Bed 34 in the recovery stage immediately above (Appendix Fig. S3). The changes in δ^{26}Mg also anti-correlate with δ^{18}O (Fig. 3). After 251.495±0.064 Ma, the δ^{13}C values of the dolomite stabilized and δ^{26}Mg values remained relatively constant at −1.6±0.2‰ (Fig. 3).

The carbonates from the YGD section have a wide span in δ^{13}C values ranging from −3‰ to 4‰ (Fig. 1C). Across the lithological boundary between the Changhsing Formation of Lopingian and the Lower Triassic Feixianguan Formation, the δ^{13}C values in carbonate show a rapid negative shift from 3.5‰ in the topmost part of the Changhsing Formation to −1‰ in the lowest part of the dolomite unit of the Feixuanguan Formation (Fig. 1C). This C isotope excursion is well correlative with the δ^{13}C excursion in most PTB sections in the Paleotethys (Cao et al., 2010; Shen et al., 2013). The carbonate δ^{13}C values above this excursion in the Lower Triassic gradually increased to 1.5‰ (Fig. 1C). Generally, the pattern and magnitude of C isotope variation in the P-T transition of YGD match the Meishan section well (Shen et al., 2013). Because low-Mg calcites are prone to resetting in terms of Mg isotope records (Hu et al., 2017; Riechelmann et al., 2016), we concentrated on the δ^{26}Mg values of dolostones across the Permian-Triassic transition. XRD analyses revealed that the d_{104} values of dolomite in the Triassic dolostones in the Yanggudong section (YGD) mostly distribute between 2.882 and 2.884 (Appendix Table S3-2), which correspond to ∼50.0 mol% $MgCO_3$ in dolomite. The dolomite δ^{26}Mg values in YGD ranged from −1.85±0.02‰ to −1.48±0.02‰ (Fig. 1C). In the P-T transition interval, dolomite δ^{26}Mg values increase slightly from −1.7% to −1.48% upward across the PTB (Fig. 1C). The variation of Early Triassic dolomite δ^{26}Mg values is within 0.1‰. The average $\delta^{26}Mg_{dol}$ of Lower Triassic is −1.67±0.15‰ ($n = 30$), well comparable with the coeval dolomite in GK-1 core (Fig. 1).

Powder XRD analyses show that the dolomite in the Dajiang section mainly occurs in the microbialite unit of the basal Daye Formation below the PTB (Fig. 1D) (Appendix Table S4). The δ^{13}C values of carbonate in the Dajiang section have been reported by Payne et al. (2004) and Wang et al. (2019). The δ^{13}C varied from 3.0‰ to −0.4‰ across the PTB and stabilized around 2.0‰ after the EPME (Fig. 1D). Dolomite consists up to 65 wt.% of the bulk carbonate rock, and the d_{104} values of dolomite range from 2.8820 to 2.8982, which correspond to 46.6-52.0 mol% of $MgCO_3$ in dolomite (Appendix Table S4). The d_{104} values of calcite in the carbonate samples mostly range from 3.023 to 3.027, corresponding to 2.6-4.0 mol% $MgCO_3$ in the calcite. The δ^{26}Mg values of bulk dolomitic limestone displayed a slight increase from −2.3‰ to −2.1‰, anti-correlative with the negative shift of carbon isotopes (Fig. 1D).

5. Discussions

Due to the diverse origins of dolomite, Mg isotope compositions in dolomite are controlled by a wide range of processes and factors (Geske et al., 2015; Higgins et al., 2018). Only if the dolomite precipitation occurred in an early marine diagenetic condition, that Mg in dolomite was sourced from contemporaneous seawater without isotopic evolution, the δ^{26}Mg values of dolomite could be used to interpret Mg isotope signatures of seawater. Therefore, a detailed understanding of the origin of the dolomite records is required before using Mg isotopes in dolomite to constrain the environmental changes during the P-T transition.

5.1. The origin of dolomite from the GK-1 core

We first concentrate on the GK-1 core, which has a complete and temporally well-constrained dolomite record over the Permian-Triassic transition. The micritic and fine crystalline textures of the dolostones are commonly inferred as the evidence for dolomite crystallization below 50 °C (Sibley and Gregg, 1987). On the other hand, the dull red luminescence of the samples under CL microscope precludes dolomitization during the burial stage. Additionally, there is no report of hydrothermal veins and faulting around the drill core site. These multiple lines of evidences suggest that dolomite from the GK-1 core formed in a syngenetic-penecontemporaneous stage (Rampino et al., 2000), and escaped overprinting of burial fluids in post-depositional stages. The trace element signatures are also supportive of syndiagenetic origin of dolomite. Redox sensitive trace elements in carbonate can be sensitive to overprinting of secondary fluids due to the low concentrations, yet a new study demonstrated that the signatures of redox sensitive trace elements in the GK-1 core faithfully recorded the anoxic to euxinic events at the time of EPME (Rampino et al., 2020), which was corroborated by U isotope records from GK-1 core itself and the temporally-equivalent sections from other localities (Zhang et al., 2020).

The early marine diagenetic origin of the dolomite is further supported by O isotope data. The pattern of the variation of δ^{18}O of the dolomite from the GK-1 drill core is consistent with the $\delta^{18}O_{apatite}$ profiles of the coeval sequences in South China (Fig. 3). Conodont $\delta^{18}O_{apatite}$ data have been widely used as a robust temperature proxy for ancient seawater due to the strong bond between O and P atoms in apatite (Chen et al., 2016; Joachimski et al., 2012). Variations in conodont $\delta^{18}O_{apatite}$ indicate remarkable increases in seawater temperature during the Permian–Triassic transition (Chen et al., 2016; Joachimski et al., 2012). $\delta^{18}O_{dolomite}$ would record surface ocean temperature because the oolitic texture in GK-1 core is indicative of a high-energy, shallow depositional environment (Boeckelmann and Magaritz, 1991; Holser et al., 1989). The consistency of the temporal patterns in $\delta^{18}O_{apatite}$ values of conodonts from many classic Permian–Triassic sections and $\delta^{18}O_{dolomite}$ values of whole-rocks from the GK-1 core indicates that the global warming event was also recorded in the carbonates (Fig. 2). Indeed, based on O isotope fractionation factors between dolomite and water (Horita, 2014), the shift in δ^{18}O from −1‰ in Permian dolomite to −4‰ in Early Triassic dolomite in the GK-1 core corresponds to a rise of >10 °C in temperature; a range that is comparable with the records of conodont $\delta^{18}O_{apatite}$ (Chen et al., 2016; Joachimski et al., 2012) and the brachiopod $\delta^{18}O_{calcie}$ (Wang et al., 2020) (Fig. 3). Therefore the petrographic, trace element and oxygen isotopic evidence collectively indicate that dolomite from the GK-1 core was formed near the sediment-seawater interface during the very early stage of diagenesis and buffered by contemporaneous seawater.

The similarity between the temporal patterns of whole-rock $\delta^{18}O_{dolomite}$ data from the GK-1 core and conodont $\delta^{18}O_{apatite}$ data further suggests that O isotopes in the dolomite from the GK-1 core have remained unaltered since deposition. In light of this, Mg isotopes in the dolomite must have remained unaltered, because O isotopic compositions and trace elements in carbonates are more susceptible to post-depositional alteration than Mg isotopes due to the high O:Mg ratio in aqueous solutions (Hu et al., 2017) and low U, Th and V contents in carbonates. In addition, Al and Ti concentrations in the GK-1 core samples are very low (Rampino et al., 2020), suggesting that Mg from detrital components has a negligible contribution to the variations of δ^{26}Mg in the dolomite. As such, the changes of δ^{26}Mg in the GK-1 core must record primary sedimentary signatures.

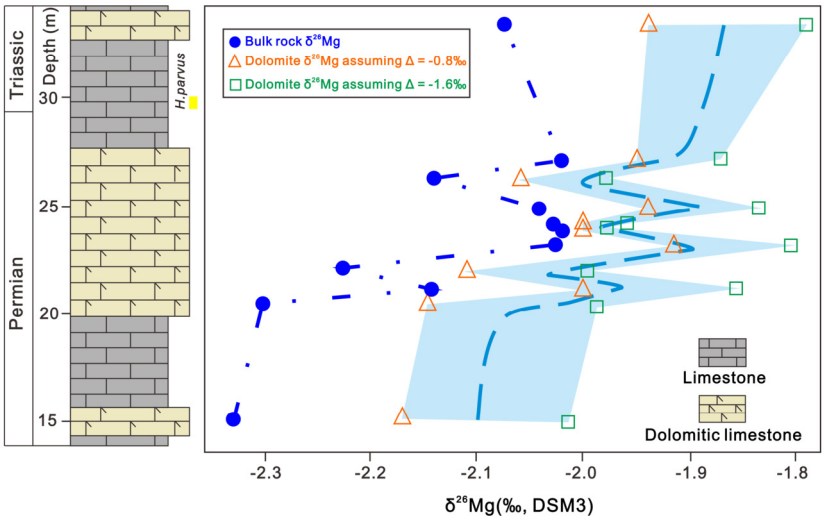

Fig. 4. Variation of lithology and Mg isotope data across the Permian-Triassic boundary in the Dajiang section.

Phanerozoic dolostones are commonly regarded as a diagenetic product that is formed via the dolomitization of calcium carbonate precursors by Mg-bearing fluids. According to reactive-transport models, dolomitization by Mg diffusion would result in a monotonic change in δ^{26}Mg values across the dolomitization front (Huang et al., 2015). However, the multiple perturbations in δ^{26}Mg in the GK-1 core do not resemble any single δ^{26}Mg profile of diffusion-driven dolomitization in reactive-transport models. It should be noted that, recently Ning et al. (2020) proposed that stratigraphic fluctuations in δ^{26}Mg in a dolostone unit could be explained by multiple dolomitization events in response to periodic sea-level oscillation. However, reflux dolomitization according to Ning et al. (2020) produces a decreasing δ^{26}Mg trend upward for a dolostone unite of 0.3 m thick, which dramatically different from the key feature of the GK-1 (i.e., an increase in δ^{26}Mg upward along >30 m thick dolostone between 220 and 250 m). Thus, the observed Mg isotopic variability in the GK-1 core was not produced by diffusion-driven dolomitization, but was caused by variations in seawater δ^{26}Mg values. Studies on modern dolomitization systems have demonstrated that platform dolomite can be seawater-buffered and possess δ^{26}Mg values in equilibrium with coeval seawater (Higgins et al., 2018). Indeed, the best explanation for the co-variations between δ^{26}Mg, δ^{18}O, and δ^{13}C along the GK-1 core is that they reflect changes in seawater composition. It would be highly fortuitous to produce the observed δ^{26}Mg changes through diagenetic processes, which also correlate with δ^{18}O and δ^{13}C signatures.

5.2. Comparison of dolomite Mg isotope records from eastern and western Paleotethys

Compared to the GK-1 core from the western Paleotethys, each of the two available carbonate sections from the eastern margin lacks thick dolomite record over the P-T boundary, nevertheless, it is possible to use multiple sections to piece together a complete dolomite record based on correlation of C isotope chemostratigraphy and biostratigraphy. Carbonates from the latest Permian interval in the Dajiang section are partially dolomitized. The dolomitized horizon is stratigraphically correlative to a large number dolomitized carbonate sections at other localities in the Tethys ocean, pointing to a large-scale dolomitization event (Li et al., 2018; Appendix Fig. S3). Such a dolomitization event was interpreted to be contemporaneous, induced by activities of sulfate reduction bacteria (Li et al., 2018). Therefore, the dolomite could record coeval seawater chemistry. And a recent study based on $\delta^{44/40}$Ca, $\delta^{88/86}$Sr, and ^{87}Sr/^{86}Sr records showed that the primary isotopic signatures of the carbonates are well preserved. Therefore it is reasonable to use Mg isotope data of dolomite from the Dajiang section to infer the Mg isotope signature of coeval seawater.

Because the carbonate samples from the Dajiang section are partially dolomitized, the measured δ^{26}Mg of the bulk samples reflect mixing of dolomite and calcite that have distinct Mg isotope compositions. The Mg isotope data for bulk Dajiang samples can be described by an isotope mass balance equation:

$$\delta_{bulk} = X_{cal} * \delta_{cal} + X_{dol} * \delta_{dol}$$

where X and δ represent the mole fraction and isotope composition of Mg in calcite and dolomite in the sample, respectively. Additionally, there is a constant Mg isotope fractionation factor between dolomite and calcite:

$$\Delta = \delta_{cal} - \delta_{dol}$$

δ_{bulk} is directly measured, X_{cal} and X_{dol} can be derived based on XRD data, and Δ is a constant. Assuming a Δ of $-0.8‰$ at a temperature of 20-30 °C based on experimental studies (Li et al., 2012, 2015), Mg isotope composition of dolomite (δ_{dol}) in each sample can be calculated combining the two equations above. As shown in Fig. 3, $\delta^{26}Mg_{dol}$ increased by 0.2‰ upward within the topmost of the Permian, from $-2.15‰$ to $-1.91‰$ (Fig. 4). Specifically, this increase in $\delta^{26}Mg_{dol}$ was concomitant with the decrease in δ^{13}C of the carbonate. It should be noted that a consensus is presently lacking on the equilibrium Mg isotope fractionation factor for Mg-bearing calcite (Li et al., 2012; Mavromatis et al., 2013). However, even if a different Δ is used, the trend in $\delta^{26}Mg_{dol}$ remains. For example, when Δ is set as $-1.6‰$ based on the studies of Mavromatis et al. (2013) and Li et al. (2015), the derived $\delta^{26}Mg_{dol}$ still demonstrate an increasing trend that anti-correlate with the δ^{13}C in the Dajiang section, increasing from $-2.01‰$ to $-1.79‰$ (Fig. 4). To conclude, regardless of the uncertainty in Δ, $\delta^{26}Mg_{dol}$ from the Dajiang section was within $-2.1\pm0.1‰$ before the negative C isotope excursion event, then increased as δ^{13}C of carbonate decreased, which are consistent with the latest Permian dolomite from the GK-1 core.

Dolomite discontinued in the Dajiang section after the P-T transition, however, the YGD section in northeast Sichuan Basin is complementary to the Dajiang section in dolomite records. The Triassic carbonates are pure dolostones whereas the Permian carbonates immediately below are limestones that show no sign of dolomitization. It should be noted that the abrupt lithological change

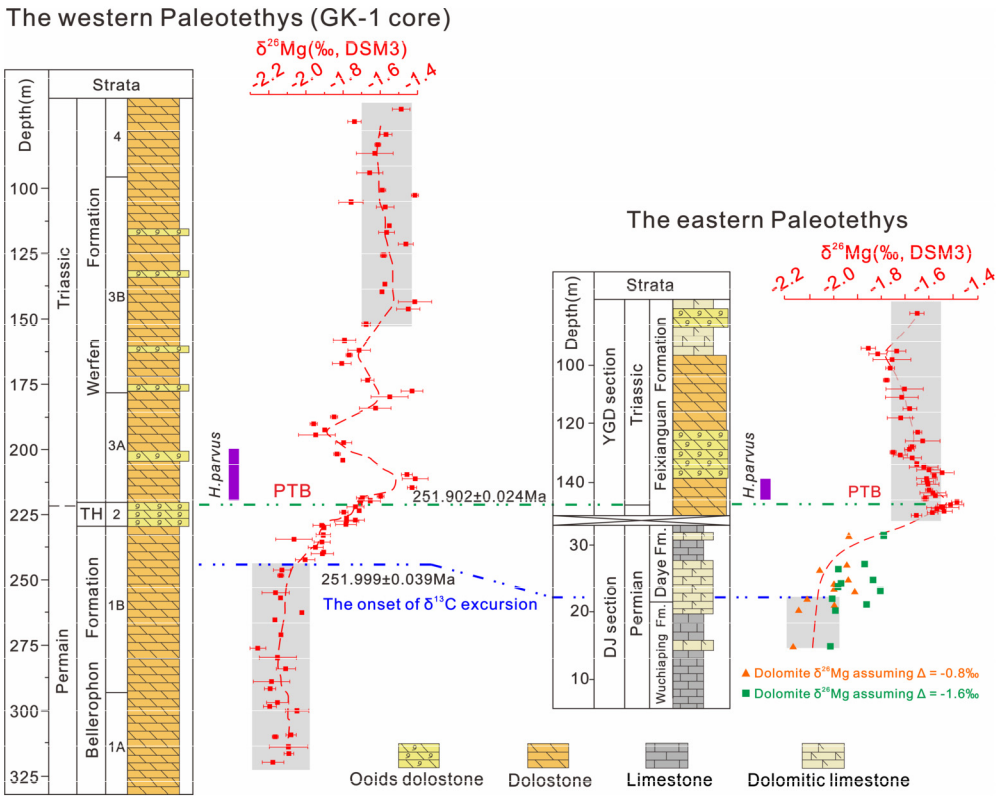

Fig. 5. A comparison dolomite δ^{26}Mg from end Permian to early Triassic for the western and eastern Paleotethys. The eastern Paleotethys section combines the record of the end Permian in Dajiang section and the record of lower Triassic in Yanggudong section.

across the Permian-Triassic boundary is a regional phenomenon rather than a random and localized feature (Wang et al., 2015). If the Triassic dolostones were formed by late diagenetic fluids, then it is difficult to explain why the underlying Permian limestone was not affected by the late dolomitization event. The best explanation is that the Triassic dolostones at the Yanggudong section was formed during the syngenetic-penecontemporaneous stage, rather than late dolomitization events. Additionally, the $^{87}Sr/^{86}Sr$ ratios of dolomicrite and fine-crystalline dolomite in the Feixianguan Formation are similar to the values of coeval seawater, inconsistent with dolomitization by late diagenetic or hydrothermal fluids (Wang et al., 2015). Thus multiple lines of evidence support that the Lower Triassic dolostones in the YGD section were formed via dolomitization in a contemporaneous-penecontemporaneous stage. Specifically, $\delta^{26}Mg_{dol}$ increases from −1.7% to −1.48% upsection across the PTB in the YGD section, which, when combined with the Dajiang section in reference to the correlative negative C isotope excursion, make up a continuous increasing trend in $\delta^{26}Mg_{dol}$ record for the eastern Paleotethys (Fig. 5). There are striking similarities between this combined $\delta^{26}Mg_{dol}$ record and the GK-1 record for the western Paleotethys as both increased from −2.1‰ in the latest Changhsingian dolomite to −1.5‰ in the Early Triassic dolomite across the PTB, and both show fluctuations after the first increase in $\delta^{26}Mg_{dol}$.

5.3. Rapid changes in seawater δ^{26}Mg during the Permian-Triassic transition

The consistent and synchronous change in δ^{26}Mg of dolostones from the three widely spaced localities, together with the mineralogical and geochemical evidence for the syndepositional nature of Mg isotope signatures in the dolostones, point to temporal changes in seawater δ^{26}Mg across the EPME. Based on the globally synchronous C isotopic anomaly in carbonates, correlative biostratigraphy, the high-precision U-Pb dates (Burgess et al., 2014) and astronomical cycles (Wu et al., 2013) for the Permian-Triassic transition at the Meishan GSSP section, as well as the well-defined astronomical cycles in the GK-1 core (Rampino et al., 2000) (Appendix Fig. S3), it is possible to place fine constraints on the temporal changes in seawater δ^{26}Mg around the EPME event based on the records in GK-1 core.

Magnesium isotope fractionation between dolomite and aqueous solution is weakly temperature dependent, with $\Delta^{26}Mg_{dolo\text{-}aq}$ varying from −1.8‰ at 20 °C to −1.7‰ at 30 °C (Li et al., 2015). Considering the fractionation factors and the temperature drifts across the PTB, the variation in δ^{26}Mg values of dolomite from the GK-1 core corresponds to a 0.4‰ shift in δ^{26}Mg values of coeval seawater, from −0.3‰ in the latest Permian to 0.1‰ in the Early Triassic. Ignoring the fluctuations in δ^{26}Mg and only considering the long-term gap between the stable periods of Lopingian and Early Triassic, the first-order rate of change in seawater δ^{26}Mg is conservatively estimated at 0.53‰ Ma^{-1} over a period of 0.75 million years (Fig. 3). However, if the fluctuations around the Permian-Triassic transition are considered, the changing rate of seawater δ^{26}Mg is ca. 3-4‰ Ma^{-1} (Fig. 3). These rates are extremely fast, indicating an extraordinarily short residence time of Mg in seawater and a tremendous disturbance in Mg cycling at such time interval. For a comparison, δ^{26}Mg of seawater varied insignificantly (within ± 0.15‰) in the last 60 million years despite the remarkable long-term changes in $^{87}Sr/^{86}Sr$ and Mg/Ca ratios in seawater over the Cenozoic (Wilkinson and Algeo, 1989).

5.4. Dolomitization and the shift in seawater δ^{26}Mg

Magnesium isotope composition of seawater is controlled by the balance between the Mg influx of riverine runoff (F_{riv}) into the ocean and the Mg outflux of dolomite precipitation (F_{dol}) and secondary Mg silicate formation ($F_{silicate}$). Mg isotope composition of

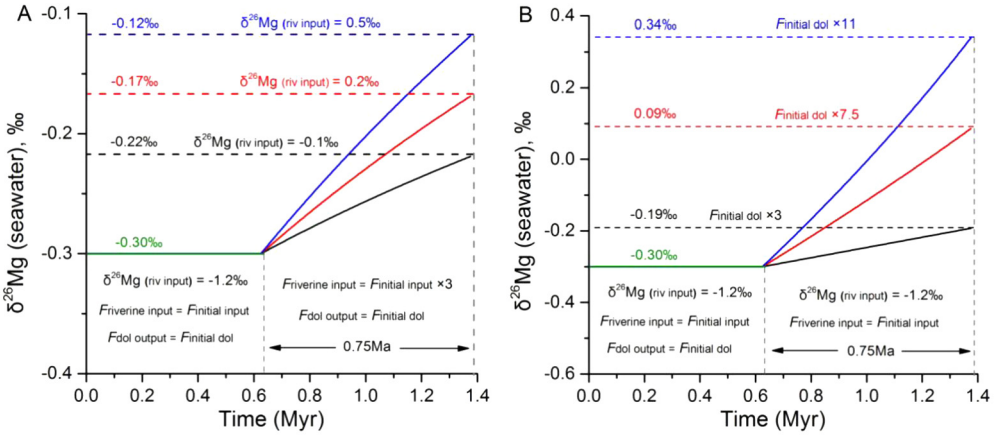

Fig. 6. Response in seawater δ^{26}Mg to (A) enhancement of continental weathering and (B) enhancement of dolomitization in oceans during Permian to Triassic transition. A steady state is assumed for seawater in Permian, and an abrupt disturbance to the steady state is induced to the box model at 0.65 Ma, to mimic the dramatic environmental changes at the end-Permian mass extinction event. Details of the model settings are provided in Appendix 3. For the scenario of enhanced continental weathering (A), δ^{26}Mg value of the riverine input is set to be −0.1‰, 0.2‰, and 0.5‰, for different scenarios; For the scenario of enhanced dolomitization (B), the dolomitization intensity is set to increase 3, 7.5 and 11 folds relative to the initial values.

seawater therefore can be modeled using an isotope mass balance equation:

$$d(\delta^{26}Mg_{sw})/dt = \delta^{26}Mg_{riv} \cdot F_{riv} - (\delta^{26}Mg_{sw} - \Delta^{26}Mg_{dol\text{-}sw}) \cdot F_{dol} - (\delta^{26}Mg_{sw} - \Delta^{26}Mg_{sil\text{-}sw}) \cdot F_{silicate} \quad (1)$$

Basalt alteration at mid-ocean ridges and formation of clay minerals in sediments are the main pathways of secondary Mg silicate formation. Alteration of basalt at high temperature is associated with quantitative Mg removal from aqueous solution, which does not produce Mg isotope fractionations in seawater (Teng, 2017). However, neoformation of clay minerals and low temperature alteration of basalts lead to removal of heavy Mg isotopes from seawater (Shalev et al., 2019). Combining these two processes, secondary Mg silicate formation is associated with close to zero or slightly positive $\Delta^{26}Mg_{silicate\text{-}seawater}$. By contrast, dolomite precipitation is associated with negative $\Delta^{26}Mg_{dolomite\text{-}seawater}$. Therefore, the increase in seawater δ^{26}Mg across the Permian-Triassic transition could be produced by enhance in dolomitization. According to Equation (1), the alternative explanation for the increase in seawater δ^{26}Mg is the increase in riverine runoffs with high δ^{26}Mg values.

It has been suggested that riverine input increased by up to 3 times as a result of soil erosion enhancement during the Permian-Triassic transition (Song et al., 2015). The effect of increased riverine input on seawater δ^{26}Mg is assessed using a box model, the details of which are provided in Appendix 3. The modeling results show that even the 3-fold increase in riverine input sustained for 0.75 million years, with a high $\delta^{26}Mg_{riv}$ value of 0.5‰, the rate of change in δ^{26}Mg for global seawater is still not fast enough to account for the observed δ^{26}Mg variations in GK-1 core (Fig. 6A). Because the increase in riverine input at the end-Permian was related to global soil erosion (Sephton et al., 2005; Song et al., 2015), such a high riverine flux should wane upon complete soil depletion, thus it is unlikely to last 0.75 million years. In addition, a $\delta^{26}Mg_{riv}$ of +0.5‰ for global average riverine input is unrealistically high, relative to the average igneous rock value of −0.25‰ (Teng, 2017). Therefore, we conclude that enhanced continental weathering alone cannot be responsible for the rapid shifts in $\delta^{26}Mg_{seawater}$ as recorded in the GK-1 core.

It has also been reported that dolomitization intensity increased remarkably at a global scale during the Permian-Triassic transition (Wilkinson and Algeo, 1989; Li et al., 2018). Modeling results indicate that in order to account for a drift of +0.4‰ for seawater δ^{26}Mg by only change of Mg outflux through dolomitization, dolomitization intensity is required to increase by a factor of 7.5 (Fig. 6B). As a result, the Mg flux ratio $[F_{dol}/(F_{dol}+F_{silicate})]$ increased from 0.5 in the Permian ocean to 0.9 in the Triassic ocean (Appendix 3), such change of Mg outflux ratio around the Permian-Triassic transition is consistent with the estimate in literature (Wilkinson and Algeo, 1989).

A compilation of the global sedimentary records for the Permian-Triassic transition illustrated remarkable higher dolomite abundance in earliest Triassic marine sediments than the late Permian sediments (Li et al., 2018), particularly around the Paleotethys ocean (Appendix Fig. S9). A number of changes in the end-Permian oceans were in accordance with the increase in dolomitization. Firstly, temperature is a well-known factor that controls the rate of dolomitization and seawater temperature increased during the Permian-Triassic transition (Chen et al., 2016; Joachimski et al., 2012), which could boost dolomitization. Secondly, dissolved sulfides have been demonstrated to catalyze dolomite precipitation (Zhang et al., 2012), and expansion of euxinic waters to shallower seafloor has also been suggested to occur during the Permian-Triassic transition (Zhang et al., 2020). In addition, microbialites and stromatolites are known as preferable for dolomitization, and the disappearance of shallow water grazers at the EPME allowed spreading of microbialites and stromatolites globally. To conclude, a significant increase in global dolomitization is a reasonable explanation for the observed first-order increase in seawater δ^{26}Mg across the Permian-Triassic transition.

5.5. Restriction events in the Paleotethys and the link to mass extinction

In the box models discussed above, a rate of 0.53‰ Ma^{-1} for the change in δ^{26}Mg for global seawater can be reproduced by significantly increasing the dolomitization intensity in oceans. However, such $\delta^{26}Mg_{seawater}$ change rate is only a conservative estimate based on the long-term trend in the GK-1 core. The Mg isotope data from dolomite interval at the PDB (i.e., 215 m-230 m of GK-1 core) requires that the change in $\delta^{26}Mg_{seawater}$ to be eight times faster (Fig. 3). It should be noted that the box model discussed above is a global ocean model, which assumes homogeneity in all seas and oceans. Evidently, such a global model would not be able to interpret the more rapid drifts in δ^{26}Mg records in the GK-1 core. In order to have a faster change in $\delta^{26}Mg_{seawater}$, the mass of the seawater in a model must be reduced to be <20% of global oceans (Fig. 7).

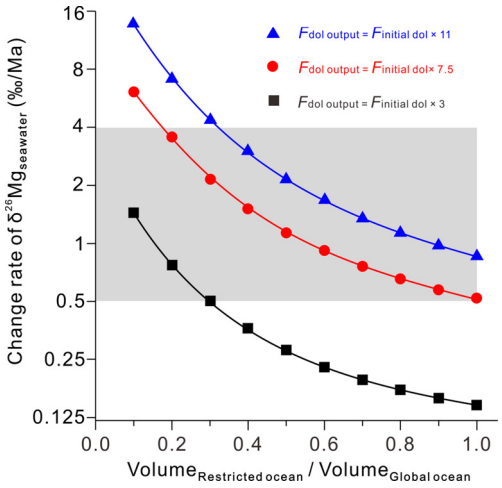

Fig. 7. The relationship between changing rate of $\delta^{26}Mg_{seawater}$, volume of the restricted ocean (basin), and intensity of dolomitization intensity according to the Mg isotope mass balance box-model, for details, see Appendix 3.

A Mg isotope study on dolostones from hinterland-attached carbonate platforms shows that $\delta^{26}Mg$ of dolomite can increase rapidly in response to basin restriction (Bialik et al., 2018) and this has been confirmed by an independent study of Ning et al. (2020). The Permian-Triassic transition was associated with a global regression event as evidenced from sedimentary disconformities in numerous sedimentary records from the oceans, particularly around the Paleotethys (Yin et al., 2014) (Appendix 4 Fig. S9). The regression event could have resulted in restriction of regional basins, where enhanced dolomitization led to rapid increase in seawater $\delta^{26}Mg$, which was recorded in the dolostones that were analyzed in this study.

It is possible that the events of restriction around the Permian-Triassic transition occurred to small local basins that were separated from each other. However, the similarity of Mg isotope patterns of the three dolomite records from the east and west of Paleotethys Ocean hints at an intriguing scenario: could the Paleotethys Ocean as a whole experienced the restriction event during the Permian-Triassic transition? Paleogeographic reconstructions suggest that the Paleotethys Ocean was surrounded by Pangea continents at 250 Ma (Fig. 1A; Appendix 3). The Paleotethys Ocean should have contained much less seawater mass than the outer Panthalassa Ocean, due to its smaller size and shallower average depth (Fig. 1A). Because shallower seawater is favorable for dolomite precipitation, dolomitization intensity should have been disproportionally higher in the Tethys than in the Panthalassa Ocean, which is indeed supported by the report of Li et al. (2018) and our own compilations (Appendix 4). Therefore, enhanced dolomitization in a restricted Paleotethys Ocean is not only supported by the multiple Mg isotope records, but also permissible from a modeling perspective (Fig. 7).

The restriction events, regardless of the scale, should have been transient, and the connection between the restricted basins and outer oceans can be restored episodically. The GK-1 core also recorded events of rapid drifts in $\delta^{26}Mg_{seawater}$ towards more negative values (Fig. 3), and this can be explained by replenish of seawater from outer oceans. It should be noted that the GK-1 core was from a continuous sequence without sedimentary hiatus, which is also consistent with the lack of detritus in the samples (Rampino et al., 2020), implying that the carbonates in the GK-1 core was supposed to have well recorded the changes in seawater chemistry without the interruption.

Magnesium isotope data therefore suggests transient periods of basin restriction within the Paleotethys Ocean around the Permian-Triassic transition, particularly, the first rapid rise of $\delta^{26}Mg_{dolomite}$ in the GK-1 core coincided with the EPME (Fig. 3). Because the mass extinction was a global event that stroke both the Paleotethys and the Panthalassa Ocean, the basin restriction was not a direct killing mechanism for the mass extinction. U isotope evidence suggests that the end-Permian oceans witnessed remarkable expansion of anoxia globally that could lead to crisis for oceanic life (Zhang et al., 2018, 2020). Restriction of the Paleotethys should have exerted a major disturbance to global seawater circulations, which might have caused stagnation of waters and subsequently development of anoxia in both the Paleotethys and the Panthalassa oceans (Hotinski et al., 2001). For organisms in the Paleotethys, the restriction event would significantly weaken the ocean's buffering capacity against external disturbances such as global warming (Chen et al., 2016; Joachimski et al., 2012), soil erosion (Sephton et al., 2005; Song et al., 2015), and enhanced dolomitization. Modeling results indicated that a 0.4‰ increase in $\delta^{26}Mg_{seawater}$ by intensified dolomitization would be accompanied by a decrease in seawater Mg/Ca ratio from 4.5 to 1.8 (Appendix 3, Fig. S8). Because skeletal marine organisms are generally adaptive to a restricted range of seawater Mg/Ca ratios (Montanez, 2002), such rapid and intensive changes in major element budgets in seawater would lead to crisis to skeletal marine life, in addition to other environmental stresses.

6. Conclusion

In this study, we report remarkable variation of $\delta^{26}Mg_{dolomite}$ values around the end-Permian extinction interval that anti-correlated with global perturbations in $\delta^{13}C_{carbonate}$ recorded from different localities in the Paleotethys. Generally, the dolomite $\delta^{26}Mg$ values displayed a first-order increase from -2.1 ± 0.1‰ at the end Permian to -1.6 ± 0.2‰ in the early Triassic. Based on the high-precision temporal model, our results suggest that the $\delta^{26}Mg$ of seawater fluctuated by 0.4‰ within ~750kyr across the Permian–Triassic transition. Modeling reveals that the high rate of change in $\delta^{26}Mg_{seawater}$ is attributed to dramatically intensified dolomitization in a relatively restricted oceanic environment. The restriction could have occurred to local basins that were separated from each other, however, our data are also consistent with a hypothesis of the Paleotethys Ocean being episodically separated from the Panthalassa Ocean around the Permian-Triassic transition. The restriction events within the Paleotethys Ocean could have significantly weakened the ocean's buffering capacity against external disturbances, and exacerbated marine environmental crisis to the marine ecosystem.

CRediT authorship contribution statement

Zhongya Hu: Sample collection, isotopic analysis, writing. **Weiqiang Li:** Project design, funding acquisition, writing. **Hua Zhang:** Sample collection, funding acquisition, revision. **Karl Krainer:** Discussion, revision, sample collection. **Quan-feng Zheng:** Sample collection, discussion. **Zhiguang Xia:** Isotopic analysis. **Wenxuan Hu:** Discussion, funding support. **Shu-zhong Shen:** Project design, funding acquisition, revision.

Declaration of competing interest

The authors declare that they have no known competing financial interests or personal relationships that could have appeared to influence the work reported in this paper.

Acknowledgements

This manuscript benefits from constructive reviews from Adrian Immenhauser and an anonymous reviewer. We thank Funing Sun

and Yaofeng Cai for the assistance to take the CL photographs. This study was supported by Strategic Priority Research Program (B) of the Chinese Academy of Sciences (Grants XDB26000000, XDB18000000), Key Research Program of Frontier Sciences, CAS (Grant QYZDY-SSW-DQC023 to SZS), and National Science Foundation of China (Grants 41473002, 41561144002 and 41622301 to WQL, and U1702242 and 41273081 to HZ).

Appendix A. Supplementary material

Supplementary material related to this article can be found online at https://doi.org/10.1016/j.epsl.2020.116704.

References

Bialik, O.M., Wang, X., Zhao, S., Waldmann, N.D., Frank, R., Li, W., 2018. Mg isotope response to dolomitization in hinterland-attached carbonate platforms: outlook of δ^{26}Mg as a tracer of basin restriction and seawater Mg/Ca ratio. Geochim. Cosmochim. Acta 235, 189–207.

Boeckelmann, K., Magaritz, M., 1991. The Permian-Triassic of the Gartnerkofel-1 core (Carnic Alps, Austria): dolomitization of the Permian-Triassic sequence. Abh. Geol. Bundesanst. (Austria) 45, 61–68.

Burgess, S.D., Bowring, S., Shen, S.Z., 2014. High-precision timeline for Earth's most severe extinction. Proc. Natl. Acad. Sci. USA 111, 3316–3321.

Burgess, S.D., Bowring, S.A., 2015. High-precision geochronology confirms voluminous magmatism before, during, and after Earth's most severe extinction. Sci. Adv. 1, e1500470.

Cao, C.Q., Yang, Y.C., Shen, S.Z., Wang, W., Zheng, Q.F., Summons, R.E., 2010. Pattern of $\delta^{13}C_{carb}$ and implications for geological events during the Permian-Triassic transition in South China. Geol. J. 45, 186–194.

Chen, J., Shen, S.Z., Li, X.H., Xu, Y.-G., Joachimski, M.M., Bowring, S.A., Erwin, D.H., Yuan, D.-X., Chen, B., Zhang, H., Wang, Y., Cao, C.-q., Zheng, Q.-f., Mu, L., 2016. High-resolution SIMS oxygen isotope analysis on conodont apatite from South China and implications for the end-Permian mass extinction. Palaeogeogr. Palaeoclimatol. Palaeoecol. 448, 26–38.

Chang, B., Li, C., Liu, D., Foster, I., Tripati, A., Lloyd, M.K., Maradiaga, I., Luo, G., An, Z., She, Z., Xie, S., Tong, J., Huang, J., Algeo, T.J., Lyons, T.W., Immenhauser, A., 2020. Massive formation of early diagenetic dolomite in the Ediacaran ocean: constraints on the "dolomite problem". Proc. Natl. Acad. Sci. USA 117 (25), 14005–14014.

Clarkson, M.O., Kasemann, S.A., Wood, R., Lenton, T.M., Daines, S.J., Richoz, S., Ohnemueller, F., Meixner, A., Poulton, S.W., Tipper, E.T., 2015. Ocean acidification and the Permo-Triassic mass extinction. Science 348, 229–232.

Fan, J.X., Shen, S.Z., Erwin, D.H., Sadler, P.M., Macleod, N., Cheng, Q.M., Hou, X.D., Yang, J., Wang, X.D., Wang, Y., Zhang, H., Chen, X., Li, G.X., Zhang, Y.C., Shi, Y.K., Yuan, D.X., Chen, Q., Zhang, L.N., Li, C., Zhao, Y., 2020. A high-resolution summary of Cambrian to Early Triassic marine invertebrate biodiversity. Science 367, 272–277.

Geske, A., Goldstein, R.H., Mavromatis, V., Richter, D.K., Buhl, D., Kluge, T., John, C.M., Immenhauser, A., 2015. The magnesium isotope (δ^{26}Mg) signature of dolomites. Geochim. Cosmochim. Acta 149, 131–151.

Higgins, J.A., Blättler, C.L., Lundstrom, E.A., Santiago-Ramos, D.P., Akhtar, A.A., Crüger Ahm, A.S., Bialik, O., Holmden, C., Bradbury, H., Murray, S.T., Swart, P.K., 2018. Mineralogy, early marine diagenesis, and the chemistry of shallow-water carbonate sediments. Geochim. Cosmochim. Acta 220, 512–534.

Holser, W.T., Schönlaub, H.P., Attrep, M., Boeckelmann, K., Klein, P., Magaritz, M., Mauritsch, H., Pak, E., Schramm, J.M., Stattegger, K., Schmöller, R., 1989. A unique geochemical record at the Permian/Triassic boundary. Nature 337, 39–44.

Horita, J., 2014. Oxygen and carbon isotope fractionation in the system dolomite–water–CO2 to elevated temperatures. Geochim. Cosmochim. Acta 129, 111–124.

Hotinski, R.M., Bice, K.L., Kump, L.R., Najjar, R.G., Arthur, M.A., 2001. Ocean stagnation and end-Permian anoxia. Geology 29, 7–10.

Hu, Z., Hu, W., Wang, X., Lu, Y., Wang, L., Liao, Z., Li, W., 2017. Resetting of Mg isotopes between calcite and dolomite during burial metamorphism: outlook of Mg isotopes as geothermometer and seawater proxy. Geochim. Cosmochim. Acta 208, 24–40.

Huang, K.-J., Shen, B., Lang, X.-G., Tang, W.-B., Peng, Y., Ke, S., Kaufman, A.J., Ma, H.-R., Li, F.-B., 2015. Magnesium isotopic compositions of the Mesoproterozoic dolostones: implications for Mg isotopic systematics of marine carbonates. Geochim. Cosmochim. Acta 164, 333–351.

Joachimski, M.M., Lai, X.L., Shen, S.Z., Jiang, H.S., Luo, G.M., Chen, B., Chen, J., Sun, Y.D., 2012. Climate warming in the latest Permian and the Permian-Triassic mass extinction. Geology 40, 195–198.

Kaczmarek, S.E., Thornton, B.P., 2017. The effect of temperature on stoichiometry, cation ordering, and reaction rate in high-temperature dolomitization experiments. Chem. Geol. 468, 32–41.

Kelley, B.M., Lehrmann, D.J., Yu, M., Minzoni, M., Enos, P., Li, X., Lau, K.V., Payne, J.L., 2017. The Late Permian to Late Triassic Great Bank of Guizhou: an isolated carbonate platform in the Nanpanjiang Basin of Guizhou Province, China. AAPG Bull. 101, 553–562.

Li, M., Song, H., Algeo, T.J., Wignall, P.B., Dai, X., Woods, A.D., 2018. A dolomitization event at the oceanic chemocline during the Permian-Triassic transition. Geology 46 (12), 1043–1046.

Li, W., Beard, B.L., Li, C., Xu, H., Johnson, C.M., 2015. Experimental calibration of Mg isotope fractionation between dolomite and aqueous solution and its geological implications. Geochim. Cosmochim. Acta 157, 164–181.

Li, W., Chakraborty, S., Beard, B.L., Romanek, C.S., Johnson, C.M., 2012. Magnesium isotope fractionation during precipitation of inorganic calcite under laboratory conditions. Earth Planet. Sci. Lett. 333, 304–316.

Ning, M., Lang, X., Huang, K., Li, C., Huang, T., Yuan, H., Xing, C., Yang, R., Shen, B., 2020. Towards understanding the origin of massive dolostones. Earth Planet. Sci. Lett. 545, 116403.

Mavromatis, V., Gautier, Q., Bosc, O., Schott, J., 2013. Kinetics of Mg partition and Mg stable isotope fractionation during its incorporation in calcite. Geochim. Cosmochim. Acta 114, 188–203.

Montanez, I.P., 2002. Biological skeletal carbonate records changes in major-ion chemistry of paleo-oceans. Proc. Natl. Acad. Sci. USA 99, 15852–15854.

Mueller, M., Igbokwe, O.A., Walter, B., Pederson, C.L., Riechelmann, S., Richter, D., Albert, R., Gerdes, A., Buhl, D., Neuser, R.D., Bertotti, G., Immenhauser, A., 2020. Testing the preservation potential of early diagenetic dolomites as geochemical archives. Sedimentology 67, 849–881.

Payne, J.L., Lehrmann, D.J., Wei, J., Orchard, M.J., Schrag, D.P., Knoll, A.H., 2004. Large perturbations of the carbon cycle during recovery from the end-Permian extinction. Science 305, 506–509.

Posenato, R., 2019. The end-Permian mass extinction (EPME) and the Early Triassic biotic recovery in the western Dolomites (Italy): state of the art. Boll. Soc. Paleontol. Ital. 58, 11–34.

Rampino, M.R., Prokoph, A., Adler, A., 2000. Tempo of the end-Permian event: high-resolution cyclostratigraphy at the Permian-Triassic boundary. Geology 28, 643–646.

Rampino, M.R., Baransky, E., Rodriguez, S., 2020. Proxy evidence from the Gartnerkofel-1 core (Carnic Alps, Austria) for hypoxic conditions in the western Tethys during the end-Permian mass-extinction event. Chem. Geol. 533, 119434.

Riechelmann, S., Mavromatis, V., Buhl, D., Dietzel, M., Eisenhauer, A., Immenhauser, A., 2016. Impact of diagenetic alteration on brachiopod shell magnesium isotope (δ^{26}Mg) signatures: experimental versus field data. Chem. Geol. 440, 191–206.

Sephton, M.A., Looy, C.V., Brinkhuis, H., Wignall, P.B., de Leeuw, J.W., Visscher, H., 2005. Catastrophic soil erosion during the end-Permian biotic crisis. Geology 33, 941.

Shalev, N., Bontognali, T.R.R., Wheat, C.G., Vance, D., 2019. New isotope constraints on the Mg oceanic budget point to cryptic modern dolomite formation. Nat. Commun. 10, 5646.

Shen, B., Dong, L., Xiao, S., Lang, X., Huang, K., Peng, Y., Zhou, C., Ke, S., Liu, P., 2016. Molar tooth carbonates and benthic methane fluxes in Proterozoic oceans. Nat. Commun. 7, 10317.

Shen, S.Z., Cao, C.Q., Zhang, H., Bowring, S.A., Henderson, C.M., Payne, J.L., Davydov, V.I., Chen, B., Yuan, D.X., Zhang, Y.C., Wang, W., Zheng, Q.F., 2013. High-resolution $\delta^{13}C_{carb}$ chemostratigraphy from latest Guadalupian through earliest Triassic in South China and Iran. Earth Planet. Sci. Lett. 375, 156–165.

Sibley, D.F., Gregg, J.M., 1987. Classification of dolomite rock textures. J. Sediment. Petrol. 57, 967–975.

Song, H., Wignall, P.B., Tong, J., Song, H., Chen, J., Chu, D., Tian, L., Luo, M., Zong, K., Chen, Y., Lai, X., Zhang, K., Wang, H., 2015. Integrated Sr isotope variations and global environmental changes through the Late Permian to early Late Triassic. Earth Planet. Sci. Lett. 424, 140–147.

Teng, F.-Z., 2017. Magnesium isotope geochemistry. Rev. Mineral. Geochem. 82, 219–287.

Wang, G., Li, P., Hao, F., Zou, H., Yu, X., 2015. Origin of dolomite in the third member of Feixianguan Formation (Lower Triassic) in the Jiannan area, Sichuan Basin, China. Mar. Pet. Geol. 63, 127–141.

Wang, J.Y., Jacobson, A.D., Zhang, H., Ramezani, J., Sageman, B.B., Hurtgen, M.T., Bowring, S.A., Shen, S.Z., 2019. Coupled $\delta^{44/40}$Ca, $\delta^{88/86}$Sr, and ^{87}Sr/^{86}Sr geochemistry across the end-Permian mass extinction event. Geochim. Cosmochim. Acta 262, 143–165.

Wang, W.Q., Garbelli, C., Zhang, F.F., Zheng, Q.F., Zhang, Y.C., Yuan, D.X., Shi, Y.K., Chen, B., Shen, S.Z., 2020. A high-resolution Middle to Late Permian paleotemperature curve reconstructed using oxygen isotopes of well-preserved brachiopod shells. Earth Planet. Sci. Lett. 540, 116245.

Wilkinson, B.H., Algeo, T.J., 1989. Sedimentary carbonate record of calcium-magnesium cycling. Am. J. Sci. 289, 1158–1194.

Wu, H., Zhang, S., Hinnov, L.A., Jiang, G., Feng, Q., Li, H., Yang, T., 2013. Time-calibrated Milankovitch cycles for the late Permian. Nat. Commun. 4, 2452.

Xie, S., Pancost, R.D., Huang, J., Wignall, P.B., Yu, J., Tang, X., Chen, L., Huang, X., Lai, X., 2007. Changes in the global carbon cycle occurred as two episodes during the Permian–Triassic crisis. Geology 35, 1083.

Yin, H., Jiang, H., Xia, W., Feng, Q., Zhang, N., Shen, J., 2014. The end-Permian regression in South China and its implication on mass extinction. Earth-Sci. Rev. 137, 19–33.

Zhang, F.F., Algeo, T.J., Romaniello, S.J., Cui, Y., Zhao, L., Chen, Z.-Q., Anbar, A.D., 2018. Congruent Permian-Triassic δ^{238}U records at Panthalassic and Tethyan sites: confirmation of global-oceanic anoxia and validation of the U-isotope paleoredox proxy. Geology 46 (4), 327–330.

Zhang, F., Xu, H., Konishi, H., Roden, E.E., 2010. A relationship between d_{104} value and composition in the calcite-disordered dolomite solid-solution series. Am. Mineral. 95, 1650–1656.

Zhang, F., Xu, H., Konishi, H., Kemp, J.M., Roden, E.E., Shen, Z., 2012. Dissolved sulfide-catalyzed precipitation of disordered dolomite: implications for the formation mechanism of sedimentary dolomite. Geochim. Cosmochim. Acta 97, 148–165.

Zhang, F.F., Shen, S.Z., Cui, Y., Lenton, T.M., Dahl, T.W., Zhang, H., Zheng, Q.F., Wang, W.Q., Krainer, K., Anbar, A.D., 2020. Two distinct episodes of marine anoxia during the Permian-Triassic crisis evidenced by uranium isotopes in marine dolostones. Geochim. Cosmochim. Acta 287, 165–179.

Zhao, R., Wu, Y.S., Jiang, H.X., Liu, Q.S., Liu, L.J., 2015. Quantitative determination constraints on dolomitization model for the Upper Permian Changxing reservoir dolomites of Northeastern Sichuan Basin, Southwestern China. Carbonates Evaporites 31, 289–305.